Two Reactivity Modes in the Heterogeneous Cyclohexene Ozonolysis under Tropospherically Relevant Ozone-Rich and Ozone-Limited Conditions

Grace Y. Stokes, Ehow H. Chen, Stephanie R. Walter, and Franz M. Geiger*

Department of Chemistry, Northwestern University, 2145 Sheridan Rd. Evanston, Illinois 60208

Received: May 3, 2009; Revised Manuscript Received: June 23, 2009

Important mechanistic differences regarding C═C double-bond oxidation processes under ozone-limited and ozone-rich reaction conditions for cyclohexene-functionalized fused silica substrates serving as model systems for studying heterogeneous C═C double bond oxidation chemistry in the troposphere are evaluated. By using broadband vibrational sum frequency generation (SFG), we track heterogeneous ozone reactions in real time. Ozone levels span three orders of magnitude and represent environments ranging from pristine remote continental regions to highly polluted urban centers, ranging from 30 ppb to 3 ppm (from 7×10^{11} molecules cm^{-3} to 7×10^{13} molecules cm^{-3}). We determine reaction rates and reactive uptake coefficients (γ values). At these tropospherically relevant ozone levels, the heterogeneous reaction rates follow a Langmuir−Hinshelwood-type mechanism. The product formation rates, which we determine as a function of ozone concentrations, are found to be half of the olefin reaction rates. This ratio is consistent with the previously proposed reaction pathway involving the breaking of one C═C double bond containing two olefinic CH moieties to form a product containing only one methyl group and one polar carbonyl moiety. Contact angle histograms show that out of a total of 60 measurements, there are about 25 more measurements with contact angles up to ten degrees below the mean recorded prior to reaction when ozone levels resemble remote continental conditions (50 ppb) than when ozone levels resemble urban conditions (1 ppm). The implication of these results are that the methyl formation pathway in heterogeneous ozonolysis may be less favorable than the carboxylic acid- and secondary ozonide-production pathway for ozone-limited conditions (i.e., in the remote continental troposphere or during urban nighttime) as opposed to ozone-rich (i.e., polluted urban atmosphere) conditions.

I. Introduction

Current worldwide emissions of mineral dust exceed 3000 Tg per year and are expected to continue to increase with expanding desertification.[1−4] Dust storms originating in the Sahara or Central Asia can carry mineral dust particles thousands of miles with weeklong lifetimes to the Americas.[5−15] While they are airborne, mineral dust particles can undergo a variety of physical and chemical transformations involving, for instance, the adsorption of semivolatile organic compounds. We have hypothesized in the past that, similar to marine surfactant coatings on sea salt aerosols,[16−18] olefin-containing organic species originating from biogenic terpene emissions by trees can coat mineral dust particles and that their heterogeneous interactions with gas-phase oxidants such as ozone drastically change the microphysics of cloud formation.[19−21] Given that biogenic VOC emissions outweigh anthropogenic emissions by a factor of 5:1, this scenario may be quite important in the troposphere.

To elucidate products and pathways important in heterogeneous ozonolysis, atmospherically relevant laboratory model systems involving straight chain olefins have been studied with great success.[22−38] These experiments provide detailed mechanistic information, reaction rates, and reactive uptake coefficients (γ values), the latter of which are of important practical use in climate models. Recently, carbonyl photochemistry has also come to the forefront as an important player in organic aerosol chemistry.[39] Vibrational sum frequency generation (SFG) has also been successfully applied to model C═C double-bond ozonolysis on aqueous surfaces.[40,41] We recently expanded the library of linear, commercially available model systems to include cyclic olefins, such as cyclohexene, cyclopentene, and limonene,[19−21] which are directly related to terpene chemistry in the troposphere. In what are the first studies of heterogeneous terpene oxidation chemistry which combine organic synthesis with the nonlinear optical spectroscopy vibrational SFG, we tracked the ozonolysis of custom-made, atmospherically relevant laboratory model surfaces to determine reaction rates and initial reactive uptake coefficients at high ozone levels ranging from 1 to 35 ppm (from 2.5×10^{13} molecules cm^{-3} to 8.7×10^{14} molecules cm^{-3}). These ozone concentrations are higher than tropospherically relevant ozone levels, which may range from 20 ppb (5×10^{11} molecules cm^{-3}) in remote locations to 500 ppb (1.2×10^{13} molecules cm^{-3}) in urban areas.[42−44] Our previous studies served as a starting point upon which we build our current work, which probes heterogeneous ozonolysis at a range of atmospherically relevant ozone concentrations, including ambient levels below 100 ppb (2.5×10^{12} molecules cm^{-3}), and which outlines important reactivity differences for ozone-rich and ozone-limited reaction conditions.

In our previous study, we reported that the ozonolysis efficiency correlates with the accessibility of the C═C double bonds at the surface. By using SFG, we characterized the surface-bound products in the CH stretching region and found substantial SFG signal increases at 2950 cm^{-1} when up to 2 ppm (5×10^{13} molecules cm^{-3}) of ozone interacts with a variety of cyclic and acyclic olefins that do not initially contain methyl groups.[19,20] This frequency is a telltale signature of a CH_3

* Corresponding author. Email: geigerf@chem.northwestern.edu, Fax: US+847-491-7713.

10.1021/jp904104s CCC: $40.75
Published on Web 07/10/2009

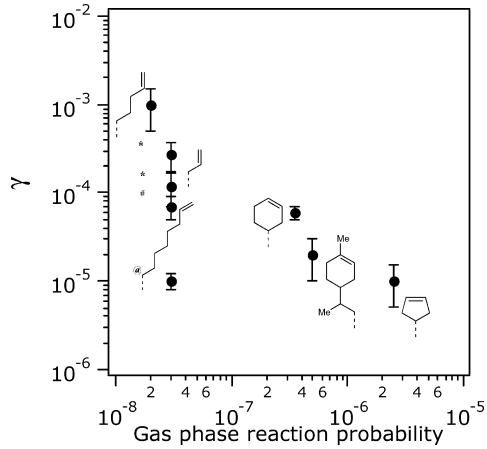

Figure 1. γ values as a function of gas-phase reaction probabilities for the ozonolysis of various olefins. Literature sources of $C3^{=}$ and $C8^{=}$ alkene γ values are denoted by shapes such that asterisks indicate values from ref 35, dagger indicates values from ref 26, and the at sign indicates values from ref 33. Cyclic olefins and linear 1-pentene γ values are reported in our previous publications (refs 19 and 21) and represented by black circles.

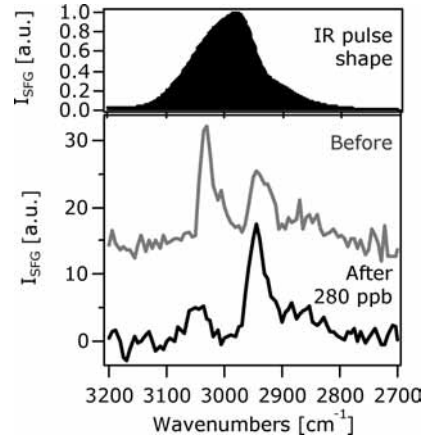

Figure 2. ssp Polarized SFG spectra obtained by adding ssp polarized SFG spectra centered at 3050 cm^{-1} and 2950 cm^{-1} and normalizing to nonresonant gold signal intensity (top, black filled spectrum).

asymmetric stretch, suggesting the formation of methyl-containing products upon C═C double-bond oxidation by ozone. The postulated reaction mechanism involves vibrationally hot Criegee intermediates producing CO_2 in the gas phase. Following a hydride shift, the products formed possibly include surface-bound methyl groups in addition to aldehydes, ketones, and carboxylic acids.[19,25,45−48] Our results complement NMR and IR studies by Rudich and co-workers,[25] Grassian and co-workers,[33] and Morris and co-workers,[49] who report spectra consistent with methyl-containing product species.[50] These studies are supported by our findings that show increases in contact angles following the oxidation of unsaturated organic species by ozone, suggesting that water uptake on mineral dust may not be promoted as previously suggested. Recently, this conclusion was also reported by Finlayson-Pitts and co-workers[51] on the basis of an impressive combination of MD simulations and IR spectroscopy.

The basic mechanism of C═C double-bond ozonolysis under homogeneous reaction conditions is well established.[52−54] However, as shown in Figure 1, the heterogeneous reaction kinetics do not follow the trends of the corresponding homogeneous reaction kinetics. The data in Figure 1 are compiled from reports on surfaces functionalized with 1-octene,[10,26,35] 1-propene,[35] amide-linked 1-pentene, cyclopentene, cyclohexene,[19,20] and ester-linked limonene[21] for similar reaction conditions. The differences may be rationalized by the notion that the spatial demands that the textbook ozonolysis mechanism places on C═C double-bond orientation dictate that the π-electron system be fully accessible to ozone from the gas phase. Ab initio calculations on the ozonolysis of isoprene support this argument.[55]

Given the strong dependence of the heterogeneous ozonolysis rates on the interfacial orientation of the C═C double bonds[19−21,32] and the unknown relationship between homogeneous and heterogeneous reaction probabilities for all but six or so terpene-related olefins (Figure 1), it is the purpose of this work to investigate the interaction between ozone at tropospherically relevant concentrations and interfaces containing a well-defined, well-characterized, well-oriented C═C double-bond system. We evaluate important mechanistic differences regarding C═C double-bond oxidation processes under ozone-limited and ozone-rich reaction conditions. The information we obtain provides chemical insight that is hopefully of use for computer models to help reduce uncertainties associated with the impact that aerosols have on climate. Specifically, we react cyclohexene-functionalized fused silica substrates with ozone concentrations that span three orders of magnitude and represent environments ranging from pristine remote continental regions to highly polluted urban centers, ranging from 30 ppb to 3 ppm (from 7 $\times$ 10^{11} molecules cm^{-3} to 7 $\times$ 10^{13} molecules cm^{-3}). Use of the cyclohexene model system allows us to carry out the reaction with a well-defined and well-characterized reactant. This model system is characterized by a relatively narrow orientation distribution (±5°) centered close to the surface normal that is rotationally invariant.[20] By probing this system with a polarization combination sensitive mainly to vibrational modes oriented along the surface normal (the ssp polarization combination), we find (Figure 2) that SFG spectra collected before (gray) and after (black) exposure to equilibrium ozone levels of 280 ppb (6.9 $\times$ 10^{12} molecules cm^{-3}) exhibit large changes in the olefinic and aliphatic CH stretch SFG signal intensities that are useful for tracking the surface-bound reactant and product species during ozonolysis in real time.

II. Experimental Section

A. Substrate Preparation and Characterization. As in our earlier work, covalently attaching cyclohexene to silica surfaces allows us to deconvolute SFG signal changes due to reaction from those due to bulk-phase evaporation and thin-film volatilization. We previously demonstrated the facile attachment chemistry and versatile synthetic modifiability of siloxane scaffolds as chemical linkers.[19−21,56−59] We continue to use silica as the inorganic substrate because it is a common mineral found in many tropospheric dust particles.[10,60] The chemistry of functionalizing silica surfaces and surfaces of related materials with organosilanes is commonly used in a variety of applications ranging from immobilizing proteins on biosensors to building novel materials.[61−72] Our cyclohexene-functionalized surfaces are prepared as described in previous publications.[19,20] Minor changes include the use of fused silica microscope slides (CGQ-0640−01, Chemglass) instead of glass slides and the use of 3-cyclohexene 1-carbonyl chloride (CAS# 932−67−2, Alfa Aesar) in place of the custom-synthesized 3-cyclohexenoyl chloride from 3-cyclohexene-1-carboxylic acid, described previously.[20] For the X-ray photoelectron spectroscopy (XPS) measurements, the analogous reactant 4-fluorobenzoyl chloride (CAS# 403−43−0, Aldrich) was used in the place of the

SCHEME 1: Surface-Functionalization Technique and Ozone Reaction[a]

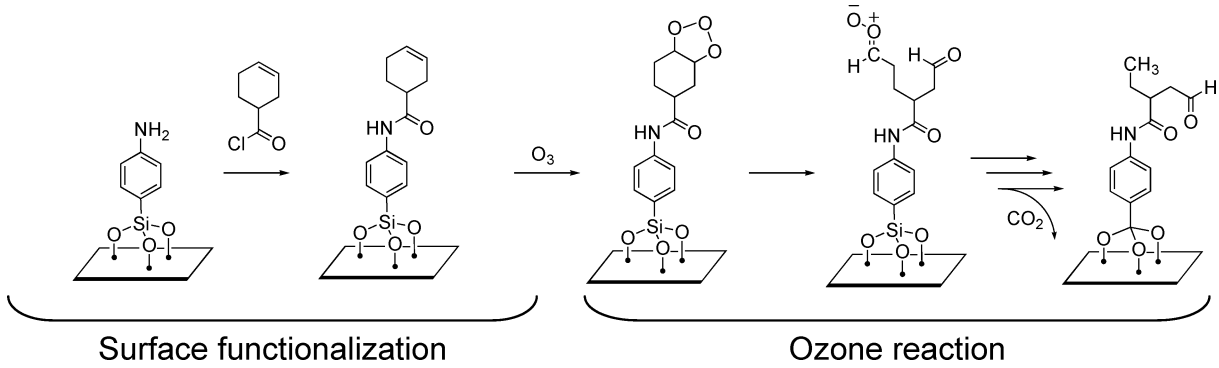

[a] Left: surface-functionalization technique for immobilizing cyclohexene by using aniline linker via amide bonding. Right: upon ozonolysis, surface-bound intermediates and products can be tracked by using surface vibrational spectroscopy. The carboxylic acid-formation pathway is omitted for clarity.

3-cyclohexene 1-carbonyl chloride and exposed to surface-bound aniline[73] under the same reaction conditions.

Characterization of cyclohexene-functionalized silica by contact angle and ellipsometry were previously published.[19,20] In the contact-angle measurements described in the current work, we use a First Ten Ångstroms (FTÅ 125) goniometer to measure sessile contact angles. XPS data show 57(5)% conversion of aniline to the amide-linked cyclohexene via an analogous reaction using 4-fluorobenzoyl chloride. XPS samples were prepared by using a Si(111) surface with a native oxide layer and cleaned and functionalized by using the same reaction conditions as those of the cyclohexene-functionalized slides. XPS measurements (Omicrometer ESCA probe, Omicrometer Nanotechnology) were referenced to C(1s) (binding energy = 284.5 eV) for each sample. F(1s) and N(1s) peaks around 685 and 398 eV, respectively, were measured with an average of three scans in 0.040 eV intervals with a dwell time of 0.200 s. The amide coupling conversion was calculated with F(1s) and N(1s) peak areas with sensitivity factors of 4.26 and 1.77 for fluorine and nitrogen, respectively.

B. Vibrational SFG and Sample Cell Description. Complete descriptions of the basis of vibrational SFG are available elsewhere,[74−81] but here, we emphasize that, unlike standard linear spectroscopies, SFG is a coherent spectroscopy.[82−84] The polarization combination used for collecting SFG spectra in this work is ssp, which denotes the polarization of the SFG, upconverter and IR light fields. As we have shown in our earlier work,[19,20] symmetry considerations lead to minimal aniline linker (Scheme 1) SFG signal intensities when the linker CH stretches are probed by using the ssp polarization. The amide linkage to the olefin of interest imparts a high degree of directionality to the covalently bound cyclohexene, which is characterized by a narrow orientation distribution centered between 0 and 24° from the surface normal.[19,20] As a key motif in Kevlar, the aniline-based amide linkage is also shown to be robust against oxidation using up to 2 ppm (5×10^{13} molecules cm^{-3}) ozone.[19,20] The two cis-configured CH moieties on the C═C double bond in cyclohexene add together constructively to yield a high olefin CH stretch intensity when using the ssp polarization.[20] Collected at ambient pressures with ten-second resolution, our SFG data provide spectroscopic and structural information to complement X-ray, AFM, and Fourier transform infrared studies. With its interface selectivity, sensitivity toward identifying adsorbed species at a small fraction of full coverage and fast, real-time data acquisition of heterogeneous processes via direct surface interrogation, broadband SFG is an excellent technique for studying ozonolysis reactions at model mineral dust surfaces.

Descriptions of our optical setup, sample chamber, and detection system are published elsewhere.[19−21,57] Briefly, we use a Spitfire Pro (800 nm, 120 fs, 2.5 mJ/pulse, 1 kHz, Spectra-Physics) laser system and an optical parametric amplifier (OPA-800CF, Spectra Physics) to produce IR radiation around 3.4 μm. The energy of the incident IR light ranges between 1 and 4 μJ per pulse with a bandwidth of $\sim$140 cm^{-1}. We clamp the substrate vertically in a custom-built, ambient-pressure Teflon gas cell and detect the SFG spectra by using a charged coupled device (CCD) camera (1340 × 100 pixels, Spec-10, Roper Scientific) after spectral dispersion (0.5 m, SP-2556, PI Acton) and optical isolation and polarization selection via the appropriate optics.[19−21,85]

The spectra we report here utilize a hybrid broadband-scanning method[86] to ensure that every vibrational mode receives appreciable IR energy over the 500 cm^{-1} region extending from 2700 to 3200 cm^{-1}. We account for the line shape and intensity of the broadband IR pulse by measuring the nonresonant SFG spectra of gold-coated glass for each IR center frequency. As described in previous publications,[19,20,57] we divide the sample SFG spectrum by the normalized nonresonant gold SFG spectrum. The individual spectra are combined, calibrated to SFG spectra of PMMA as described previously,[57] and normalized to produce the spectra shown in Figure 2. These spectra are background-subtracted averages of seven collections each acquired within 30 s. Background spectra are acquired by blocking the IR input, thus accounting for optical scattering from the 800 nm upconverter. Note that the SFG E-field does not only depend on the number density of oscillators located at the interface but also on their molecular orientation.

The method by which we generate ppb ozone levels was described in previous publications.[19−21] All experiments were carried out at a total pressure of 1 atm. By minimizing the path length of Teflon tubing through which oxygen, helium, and ozone gases travel and by diluting with helium both before oxygen gas enters the Hg pen ray lamp (90−0004−01, UVP) and before ozone gas enters the Teflon sample chamber, we generated the 30 ppb to 3 ppm (7×10^{11} to 7×10^{13} molecules cm^{-3}) initial ozone levels reported in this work. We enhanced the signal-to-noise ratio of our UV−vis spectrometer (USB4000E, 185−850 nm, Ocean Optics) by averaging ten data acquisitions and applying a boxcar function to the absorbance data collected at 254 nm. At the beginning of each experiment, we allowed the Hg pen ray lamp to warm up for approximately 30 min while flowing ozone gas across a dummy glass slide in the reaction chamber and detecting the UV−vis absorbance of the ozone gas that exits the sample chamber. Subsequently, we

turned off the lamp for 30 min and purged the tubing and chamber with helium and oxygen gas. Next, we placed the cyclohexene-functionalized silica substrate into the Teflon chamber. We flowed helium and oxygen gases through the chamber across the functionalized silica sample for 10 min while simultaneously collecting SFG spectra and measuring UV−vis absorbance at 254 nm in-line. Then, we turned on the Hg pen ray lamp and identified the time ozone reaches the sample as $t = 0$ min in the time traces shown in this work.

III. Results and Discussion

A. Vibrational SFG Spectra. When cyclohexene reacts with ozone, the textbook mechanisms[52−54,87] indicate that the primary ozonide and its two decomposition fragments, a Criegee intermediate and an aldehyde, shown in Scheme 1, should remain surface-bound to allow spectroscopic characterization of intermediate and product species using SFG. In Scheme 1, we omit the carboxylic acid pathway, which is well established[19,24,25,28,33,35,49,50,88−90] for heterogeneous and homogeneous reaction conditions, for clarity. We expect to observe a decrease in the SFG signal intensity of the olefinic CH stretch and changes in SFG signal intensities of the aliphatic CH stretches because of reorientation of the methylene groups along the carbon chain.[53,54,87,88,90,91] Our previously suggested reaction mechanism for the heterogeneous ozonolysis of cyclohexene[19] includes a pathway producing methyl-containing alkane products. Therefore, we expect SFG signal intensity at the frequencies associated with methyl asymmetric stretch modes (2940−2950 cm^{-1}) to correspond to methyl product formation.[19] Secondary ozonide products have been suggested to contribute vibrational signatures in this frequency range as well.[50]

We assign the vibrational modes in our spectra shown in Figure 2 according to literature values.[20] Prior to ozone exposure (top, gray trace), a strong vibrational mode is present at 3030 cm^{-1}, which we assign to the olefinic CH stretch.[20] Upon ozonolysis by 280 ppb ozone (6.9×10^{12} molecules cm^{-3}), we find that the SFG signal intensity due to the olefinic CH stretch at 3030 cm^{-1} is diminished (bottom, black trace), whereas the SFG signal intensity at 2940 − 2950 cm^{-1} increases.

In our coherent spectroscopies, the SFG signal intensity is the square modulus of the sum frequency E-field (E_{SFG}), which is proportional to the number density of surface-bound species. Yet, the SFG E-field does not only depend on the number density of oscillators located at the interface but also on their molecular orientation. Although we cannot completely rule out that the rise of the SFG E-field at 2940 cm^{-1} following ozone exposure is due to molecular reorientation of a methylene group in the strained cyclohexene ring as opposed to C=C double ozonolysis, our published work on the ozonolysis of cyclopentenyl-, *n*-pentenyl-, and menthenoyl-functionalized surfaces all exhibit the same spectral signature at 2940 cm^{-1} following ozone exposure.[19−21] On the basis of detailed polarization-resolved SFG studies for the surfaces before and after ozonolysis,[20] we attribute the SFG E-field change to C=C double-bond ozonolysis.

In Figure 3A, we plot the ratio of the SFG E-fields at 2940 cm^{-1} after ozone exposure to the SFG E-fields at the same frequency before ozone exposure for initial ozone levels ranging up to 7×10^{13} molecules cm^{-3}. To accommodate variations in cyclohexene surface coverage, the spectra were normalized to the SFG signal intensity due to the olefinic CH stretch before exposure to ozone. We find that this ratio changes by a factor of up to two when the surfaces are exposed to up to 2×10^{13} molecules cm^{-3} ozone and then remains above 1.3 for higher ozone concentrations. The data shown in Figure 3A are consistent with the hypothesis that the number of methyl groups produced from ozonolysis increases with ozone partial pressures up to 2×10^{13} molecules cm^{-3} ozone. Above 2.5×10^{13} molecules cm^{-3} ozone, the SFG E-field ratios at 2940 cm^{-1}, which report on methyl group formation, become much less dependent on ozone concentration. This finding suggests surface site saturation by ozone and a cessation in the net production of methyl groups with increasing ozone concentration or orientational scrambling.

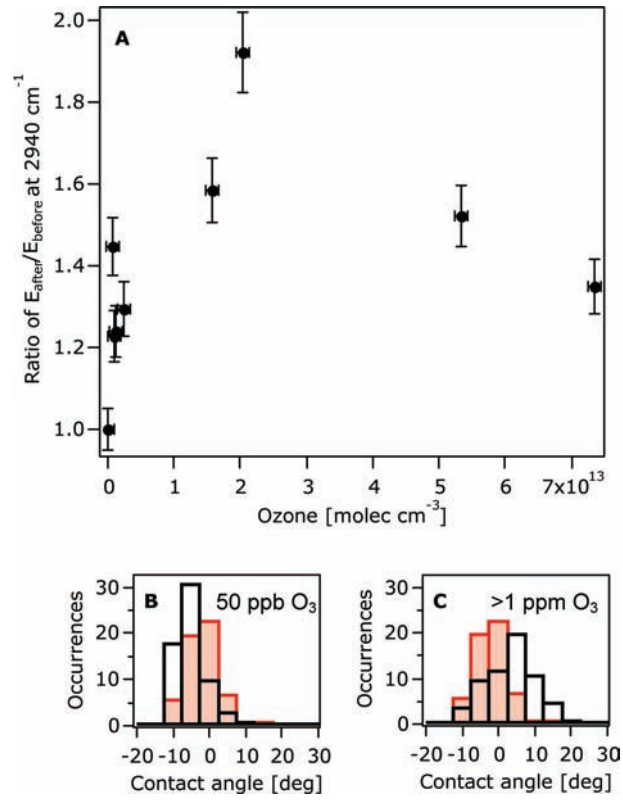

Figure 3. (A) Ratio of E_{SFG} for asymmetric stretch at 2940 cm^{-1} before and after exposure to ozone levels ranging up to 7.3×10^{13} molecules cm^{-3}. Contact-angle distribution before (shaded gray bars) and after (bars outlined in black) exposure to (B) 1×10^{12} molecules cm^{-3} (50 ppb) or (C) over 2×10^{13} molecules cm^{-3} (over 1 ppm) ozone levels.

B. Contact Angle Measurements. Contact angle measurements taken before and after exposure to ozone are a function of the hydrophobicity, net polarity, and net orientation of surface-bound product species. In this study, these measurements serve as a macroscopic indicator of the extent of methyl-containing alkane product formation. To quantify the subtle changes in the measured contact angles, we analyzed the distributions of the contact angle before (filled gray bars) and after (empty black bars) exposure to 50 ppb (1×10^{12} molecules cm^{-3}, Figure 3B) and over 1 ppm (2.5×10^{13} molecules cm^{-3}, Figure 3C) ozone levels. Our data include 60 measurements each for before and after each concentration of ozone,[19] and the distributions are binned by the same four-degree increments. Both histograms are centered at the mean contact angle obtained before exposure to ozone and plotted as deviations from the pre-ozone mean value. Upon exposure of the surface to 1×10^{12} molecules cm^{-3} ozone, the contact angle distribution shifts to lower values by 5−10 degrees (Figure 3B). In comparison, Figure 3C shows that the contact angle distribution shifts to higher values by the same amount when the surface is exposed to 2.5×10^{13} molecules cm^{-3} ozone.

The contact angle histograms show that out of a total of 60 measurements, there are about 25 more measurements with contact angles up to ten degrees below the mean recorded prior to reaction when ozone levels resemble remote continental conditions (50 ppb) than when ozone levels resemble urban conditions (1 ppm). These results can be correlated to the ones we obtained for pre- and post-ozone exposure SFG E-field ratios at 2940 cm^{-1}, which cover the same ozone levels. Recall that we showed the SFG E-field ratios at 2940 cm^{-1} to increase with ozone concentrations, suggesting higher methyl surface coverages (Figure 3A). This finding is consistent with the increases in contact angles that we observe here for 2.5×10^{13} molecules cm^{-3} of ozone, as higher contact angles indicate a more hydrophobic surface (Figure 3C). At low ozone concentrations (1×10^{12} molecules cm^{-3}), the product species include fewer methyl groups (Figure 3A), and the ozonolysis results in a less hydrophobic surface (Figure 3B). Note that the contact angles for cyclohexene-functionalized substrates before exposure to ozone ranged from 48 to 52°, which was incorrectly reported as 36° in the text of our previous publication but correctly shown in its corresponding figure.[19]

C. Ozone-Rich and Ozone-Limited Reaction Conditions. Together with the SFG results presented in the previous section, we suggest that under ozone-limited conditions (below 1 ppm or 2.5×10^{13} molecules cm^{-3}), the methyl formation pathway may be less favorable than the carboxylic acid- and secondary ozonide-production pathway. Under ozone-rich conditions (above 1 ppm or 2.5×10^{13} molecules cm^{-3}), we observe spectral evidence of more methyl-containing products. The maximum methyl-group yield is found right at 2.5×10^{13} molecules cm^{-3} ozone. Note that small amounts of OH radical formation[89,92−94] at high ozone concentrations may cause oligomerization[95,96] or hydrocarbon degradation,[97] which we expect to become important if the ozone concentration is sufficiently high.

D. Monitoring Ozonolysis in Real Time. In our flow setup, the initial ozone concentrations are a function of the gas flow rates, which vary with backpressures in our helium and oxygen gas tanks. For example, although the final ozone concentration equilibrates at 6.9×10^{12} molecules cm^{-3}, the initial ozone level after 30 s of flow is 100 ppb (2.5×10^{12} molecules cm^{-3}). In our kinetic analysis below, we use the ozone concentrations recorded at 30 s instead of those reached under steady-state conditions because cyclohexene reacts with minute-long half-life times.[19] We also observed that when we introduced 2 ppm (5×10^{13} molecules cm^{-3}) levels of ozone for only a few seconds, the reaction takes place to the same extent as when we exposed cyclohexene to 5×10^{13} molecules cm^{-3} levels of ozone for 30 min or more.[19]

With ten-second resolution, we track the changes in the SFG E-field of the olefin stretch at 3030 cm^{-1} and the asymmetric stretch at 2940 cm^{-1} during ozone exposure. Note again that the SFG E-field is proportional to the number of oscillators at the surface, that is, the number of C═C double bonds present at the interface. After referencing the SFG E-field to zero and normalizing to one for each vibrational mode of interest, we fit the SFG E-field versus time trace to a first-order exponential ($E_{SFG} = A + Be^{-\text{rate}\times\text{time}}$) to obtain the reaction rate. To fit the SFG E-field corresponding to the reactant disappearance over time, we held A at 0 and B at 1, whereas A was held at 1 and B was held at −1 to fit the SFG E-field associated with product formation over time. Figure 4A−D shows changes in SFG E-fields at 3030 and 2940 cm^{-1} as cyclohexene-functionalized surfaces were exposed to four different ozone concentrations ranging from 40 ppb (9×10^{11} molecules cm^{-3}) to over 800 ppb (2×10^{13} molecules cm^{-3}) initial ozone levels (which correspond to 65 ppb to 1.8 ppm or 1.5×10^{12} molecules cm^{-3} to 4.4×10^{13} molecules cm^{-3} equilibrium ozone levels). In all four panels, the SFG E-field corresponding to the olefinic CH stretch decays, whereas the SFG E-field corresponding to the methyl asymmetric CH stretch increases. At the two lowest ozone concentrations (Figure 4A,B), the rates of both methyl-product formation and olefin disappearance are smaller than the rates observed for high ozone levels in Figure 4C,D.

Figure 5A shows how the reactant-consumption and product-formation rates depend on the ozone concentration. Clearly, the reaction between surface-bound cyclohexene and gas-phase ozone exhibits self-limiting behavior, which is reminiscent of a Langmuir−Hinshelwood-type dependence on the gas-phase ozone concentration. Note that Langmuir−Hinshelwood theory[98−102] requires both reactants to be adsorbed to the surface from the gas phase. Because our surfaces that are presented to the incoming ozone molecules are already functionalized with olefins when the reaction begins, Langmuir−Hinshelwood theory does not, strictly speaking, apply. Nevertheless, here, we follow Finlayson-Pitts and co-workers,[35] who, along with Poeschl et al.,[103] Kwamena et al.,[104] McNeill et al.,[105] and Mmereki and Donaldson,[106] invoked this mechanism for linear olefins. In the Langmuir−Hinshelwood mechanism, gas-phase ozone is in equilibrium with adsorbed ozone molecules, and then, the interaction with the surface-bound C═C double bond occurs. Thus, surface-bound cyclohexene will only react when ozone is adsorbed onto the surface.[98] Provided that the number of ozone-binding sites is limited, we expect that a certain gas-phase ozone concentration will result in surface saturation, at which point the reaction rate levels off and becomes independent of ozone concentration. Figure 5A shows that this is indeed observed not only for the olefin reactant but also for the product species, which we interpret to be a methyl group. Over the ozone concentration range covered in this work, the alternative surface reaction mechanism, which follows that first proposed by Eley and Rideal,[107] is not operative. In this mechanism, the gas-phase species reacts directly with a surface-localized reaction partner without the need for prior adsorption. The reaction rates are thus linearly dependent on ozone concentrations until a maximum rate is reached when all surface-bound reactants are consumed, after which the reaction rate decays back to zero for high gas-phase reactant levels.[99] Over the ozone concentration covered in this work, this effect is clearly not observed.

Following Kwamena et al., we fit our data to eq 1, a modified version of the Langmuir equation:[36]

$$\text{rate}_{obs} = \frac{k^{I}_{max} K_{O_3}[O_3(g)]}{1 + K_{O_3}[O_3(g)]} \quad (1)$$

Here, rate_{obs} is the measured rate in s^{-1}, $[O_3(g)]$ is the gas-phase ozone concentration in molecules per cm^3, K_{O_3} is the ozone gas-to-surface equilibrium constant, and k^{I}_{max} describes the pseudo first-order rate that would be observed at high ozone concentrations and that is equivalent to the product of k_s, the second-order surface rate coefficient (vide infra), and the number of surface sites. The following best fit parameters for olefin disappearance as a function of ozone concentration were obtained: $k^{I}_{max} = 4.4(4) \times 10^{-2}$ s^{-1} and $K_{O_3} = 1.8(8) \times 10^{-13}$ cm^3 $molecules^{-1}$. Likewise, the best fit parameters for increases

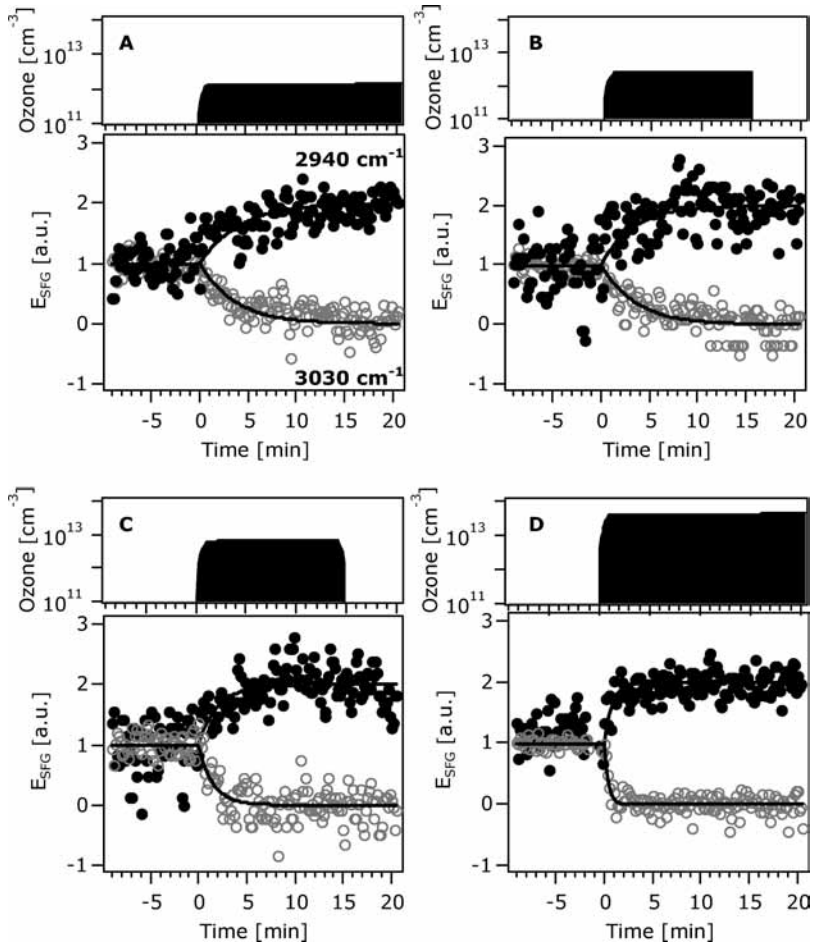

Figure 4. Real time monitoring of ozone and E_{SFG} at 3030 cm^{-1} (gray empty circles) and 2940 cm^{-1} (black filled circles) during exposure to equilibrium ozone levels ranging from 1.5×10^{12} molecules cm^{-3} (A), 2.5×10^{12} molecules cm^{-3} (B), 6.9×10^{12} molecules cm^{-3} (C), and 4.4×10^{13} molecules cm^{-3} (D), which correspond to initial ozone levels of 9×10^{11} molecules cm^{-3}, 1.3×10^{12} molecules cm^{-3}, 2.5×10^{12} molecules cm^{-3}, and 2×10^{13} molecules cm^{-3}, respectively. Ozone levels are shown on a log scale (top, black filled spectra) for corresponding E_{SFG} traces.

in SFG E-field at 2940 cm^{-1}, indicating product formation, were $k^{I}_{max} = 2.3(2) \times 10^{-2}$ s^{-1} and $K_{O_3} = 2.7(3) \times 10^{-13}$ cm^3 molecules^{-1}. In Figure 5A, k^{I}_{max} is graphically represented by the asymptote. At ozone concentrations higher than 2×10^{13} molecules cm^{-3}, the rates for both the olefinic CH stretch disappearance and the methyl asymmetric stretch appearance become independent of ozone concentration. The k^{I}_{max} values we determined for the olefin stretch disappearance and product formation are similar to the k^{I}_{max} value reported for reactions between ozone and anthracene adsorbed on hexanoic acid[106] but one order of magnitude smaller than the rate reported for ozonolysis of anthracene on silica.[36] The K_{O_3} values we observe, which describe the partitioning of ozone to cyclohexene-functionalized silica, are two orders of magnitude smaller than the rate reported for ozonolysis of anthracene on silica[36] and one order of magnitude smaller than the equilibrium constants reported for ozone interactions with anthracene on water, stearic acid, or hexanoic acid.[106]

To further quantify the relationship between the rate of reaction and methyl production, we plotted the olefin reaction rate as a function of the methyl formation rate (Figure 5B). Within experimental uncertainty, the product formation rate depends linearly on the reaction rate at low ozone concentrations (slope = 1.8(3), two gray guidelines are included in Figure 5B to denote the high and low boundaries of the relationship between olefin disappearance and product formation). The slope we obtain from the data in Figure 5B is consistent with the 2:1 ratio of the reactant disappearance rate to the methyl product formation rate determined from the data shown in Figure 5A for ozone levels above 0.8 ppm or 2×10^{13} molecules cm^{-3}. In addition, these results are consistent with the reaction pathway summarized in Scheme 1: each cyclohexene moiety undergoing ozonolysis begins the reaction with two olefinic CH groups but ends with one methyl group. Because the SFG E-field scales with number density of species on the surface, the rate of olefinic CH stretch disappearance is expected to be twice as fast as the rate of methyl-containing product formation (shown in Scheme 1). Again, only half of the branched products will contain a methyl group, whereas the other half will contain an aldehyde, ketone, or carboxylic acid group. This mechanistic interpretation is supported by the number density of methyl-containing product species quantified in Figure 3A, such that under ozone-rich conditions (above 0.8 ppm or 2×10^{13} molecules cm^{-3}), we observe a high number density of methyl-containing product species. At these same high ozone concentrations, the rate of formation of product species levels off at a slower rate than the rate of disappearance of the olefinic stretch.

E. γ Values. To connect our laboratory measurements to global circulation models, we calculate the reactive uptake coefficient, or the ratio of surface reactions to collisions,[108] for

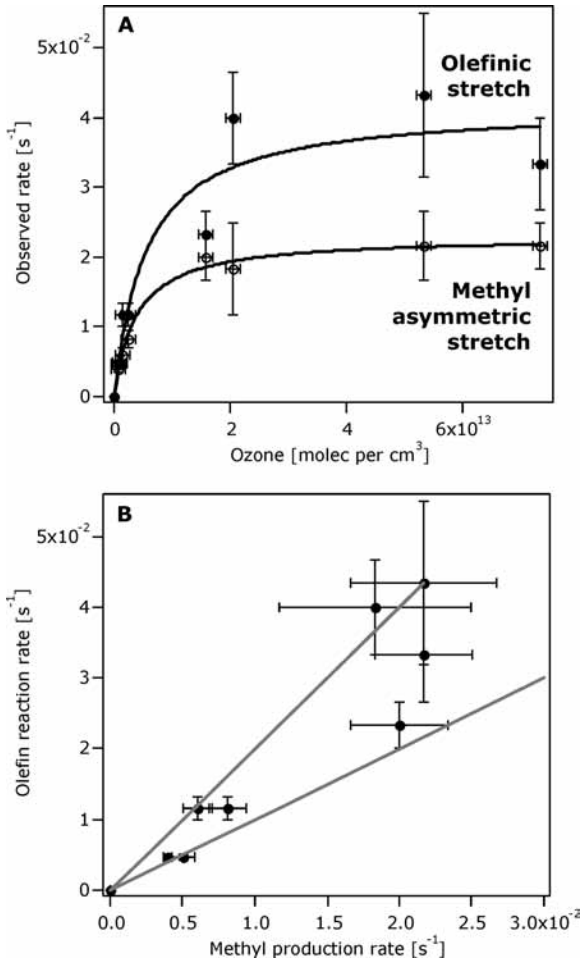

Figure 5. (A) Observed rates of decrease in olefinic stretch at 3030 cm^{-1} and increase of methyl asymmetric stretch at 2940 cm^{-1} at corresponding initial ozone levels. (B) Olefinic reaction rate compared to methyl production rate with lines (slopes = 2 and 1) as guides to the eye.

the interaction of ozone with our cyclohexene-functionalized surface by using the following expression in eq 2:

$$\gamma = \frac{\mathrm{d}[\Delta E_{\mathrm{SFG}}]}{\mathrm{d}t}\bigg|_{t=t_{\mathrm{rxn}}} \frac{[\mathrm{terpene}]_{0,\mathrm{surface}}}{\Delta E_{\mathrm{SFG},t=\infty}[\mathrm{O_3}]\sqrt{RT/2\pi M}} \qquad (2)$$

Descriptions of the method we used to calculate γ values follow the pioneering work of Dubowski et al.[35] and are found in our previous publications[19,21] for the case of SFG. A key difference in our current work is the different value used for initial surface-bound terpene concentration, $[\mathrm{terpene}]_{0,\mathrm{surface}}$. Previously, γ values (such as those shown in Figure 1) were calculated with a $[\mathrm{terpene}]_{0,\mathrm{surface}}$ of 3×10^{14} molecules cm^{-2}. This value is based on the total number of possible sites on silica, 1×10^{15} cm^{-2}, and assumed 100% conversion of the full coverage of aminophenyl trimethoxy silane species, corresponding to 3×10^{14} C=C double bonds cm^{-2}.[73] However, in the XPS experiments using our fluorine tag (vide supra), we observe that about half of these aniline sites are converted to amide-linked cyclohexene functional groups. Therefore, the current, more conservative, estimate we use for $[\mathrm{terpene}]_{0,\mathrm{surface}}$ to calculate the γ values shown in Figure 6 is 1.5×10^{14} molecules cm^{-2}. The γ values obtained here are somewhat smaller than those reported by Hearn and Smith

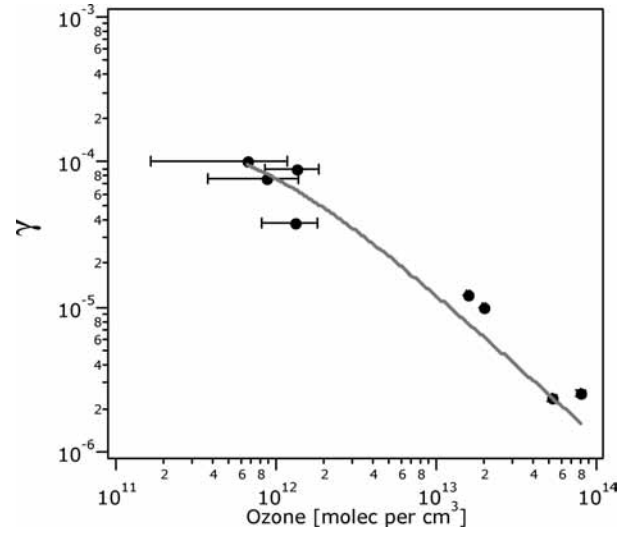

Figure 6. γ values versus ozone concentration follow a Langmuir–Hinshelwood relationship.

for oleic and linoleic acid as well as oleyl alcohol and 1-octadecene (10^{-3} to 10^{-4} range)[30] and those reported by Knopf et al. for multicomponent liquid oleic acid mixtures (10^{-4} to 10^{-5} range).[109]

We also calculated $(\mathrm{d}[\Delta E_{\mathrm{SFG}}])/(\mathrm{d}t)$ by using the first derivative $(\mathrm{d}[\Delta E_{\mathrm{SFG}}])/(\mathrm{d}t) = -\mathrm{rate} \times \mathrm{e}^{-\mathrm{rate}\times\mathrm{time}}$ at $t = 30$ s. The correlation between γ values and ozone concentrations can be fit by using the parametrization described in our previous work.[19,21] The Langmuir–Hinshelwood relationship between γ value and ozone concentration involves the variables k_s, the second-order rate constant, and B, the surface-accommodation coefficient, also called the sticking or trapping probability.[35,100] B corresponds to the ratio of the desorption rate constant to the adsorption rate constant.[35,100] The best fit value for k_s for cyclohexene is $1.4(7) \times 10^{-17}$ cm^2 $molecules^{-1}$ s^{-1} which is similar to the k_s value of 2×10^{-17} cm^2 $molecules^{-1}$ s^{-1} reported by Dubowski et al.[35] for ozonolysis of a terminal alkene functionalized silica surface. The B value of $6(1) \times 10^{11}$ molecules cm^{-3} observed in the current work is two orders of magnitude smaller than the B value reported by Dubowski et al.[35] (4×10^{13} molecules cm^{-3}), which suggests ozone interacts more strongly with cyclohexene than with a terminal vinylic alkene group. This is not surprising because the γ value we calculate for cyclohexene is higher than the γ values Dubowski et al.[35] reported for $C_8^=$ or $C_3^=$ alkene silanes. Likewise, our B values is slightly smaller than the B value reported for benzo-[a]pyrene (BaP)-coated soot[38] and that reported for oleate in submicrometer aqueous salt aerosols studied by McNeill et al.,[105] and much smaller than B values for anthracene adsorbed on water or octanol[106] or BaP on organic particles.[104]

IV. Implications for Tropospheric Chemistry–Reactivity under Urban Versus Remote and Daytime Versus Nighttime Conditions

In this work, SFG is used to study well-defined, well-oriented, cyclic olefin systems covalently attached to silica and to determine reaction rates and γ values for tropospherically representative ozone concentrations. Similar to work by Finlayson-Pitts and co-workers,[35] who studied terminal alkenes, we find that ozone reaction rates for cyclohexene follow a Langmuir–Hinshelwood-type mechanism. Our SFG studies also show that the product formation rates, which we determine as a function of ozone concentrations, are half of the olefin reaction

rates. This ratio of 1:2 in the rates is consistent with the proposed reaction pathway we reported previously,[19] where one C═C double bond containing two olefinic CH moieties reacts to form a product containing only one methyl group. The extent to which methyl-containing products form strongly depends on the ozone concentration. Specifically, the SFG studies together with contact angle measurements suggest that under ozone-limited conditions (below 1 ppm or 2.5×10^{13} molecules cm^{-3}, representative of the remote continental atmosphere), the methyl-formation pathway may be less favorable than the carboxylic acid- and secondary ozonide-production pathway. Under ozone-rich conditions (above 1 ppm or 2.5×10^{13} molecules cm^{-3}, representative of the polluted urban atmosphere), we observe spectral evidence of more methyl-containing products, and the maximum methyl group yield is obtained at 1 ppm or 2.5×10^{13} molecules cm^{-3} ozone.

Insofar as these laboratory studies are representative of real world environments, including heterogeneous reactions of mineral dust containing unsaturated semivolatile organic compounds as complex as humic-like substances,[110] our findings indicate that aerosol particle surfaces are likely to be armed with nonpolar organic groups such as methyl groups if ozone levels are sufficiently high during the day. Under this scenario, other steps, most likely reactions with OH radicals, need to be considered for a polarity switch toward more hydrophilic surfaces to occur. Under remote conditions, where the ozone concentration in the gas phase is substantially lower, or during the urban night, organic-coated surfaces are fully expected to switch their polarity and increase their propensity to interact with water vapor.

V. Future Work

In the future, we plan to fully characterize the polar product species of heterogeneous ozonolysis by acquiring SFG spectra in the C═O stretching region. At low ozone levels, we expect the rate of C═O formation to be directly proportional to the olefin reaction rate and the methyl product formation rate. We will also measure gas-phase products with our chemical ionization mass spectrometry system, which was previously used to study interactions between indoor air pollutants and titanium dioxide-coated silica surfaces.[111,112] Our cyclohexene work opens up heterogeneous oxidation studies on more ring-strained or less ring-strained cyclic alkenes as well as mixtures of two or more unique species to help increase the complexity of our model systems toward increasingly realistic mimics of biologically relevant VOCs. Studying the heterogeneous oxidation of our vast library of organic-functionalized surfaces[113] which include biologically relevant chiral and achiral reactants such as sugars and DNA[57−59] with other oxidants such as NO_2, OH, and HNO_3 will extend our laboratory model system to more chemically diverse, realistic models of inorganic and organic aerosols, including mineral dust. We will also expand the parameter space of the gas-phase conditions to include varying relative humidity and temperature. We plan to monitor surface-bound intermediates and elucidate reaction pathways by freezing out reactive intermediates and by using isotope-labeled substrates to monitor kinetic isotope effects. These studies will enable a deeper chemical understanding of complex heterogeneous oxidation processes, which, in turn, will contribute to bridging the gap between laboratory model systems and field studies.[110]

Acknowledgment. G.Y.S. gratefully acknowledges support from NASA Headquarters under the NASA Earth and Space Science Fellowship program (Grant 08-Earth08R-0049). S.R.W. acknowledges support from a William Banoff Fellowship. We gratefully acknowledge support for this work from the National Science Foundation Atmospheric Chemistry division (Grant NSF ATM-0533436). XPS was performed in the Keck II facility of the NUANCE Center at Northwestern University. NUANCE Center is supported by NSF-NSEC, NSF-MRSEC, Keck Foundation, the State of Illinois. and Northwestern University. The authors also acknowledge donations, equipment loans. and the technical support of Spectra Physics, a division of Newport Corporation.

References and Notes

(1) Laurent, B.; Marticorena, B.; Bergametti, G.; Leon, J. F.; Mahowald, N. M. *J. Geophys. Res.* **2008**, *113*.

(2) Michel, A. E.; Usher, C. R.; Grassian, V. H. *Atmos. Environ.* **2003**, *37*, 3201.

(3) Xuan, J.; Sokolik, I. N. *Atmos. Environ.* **2002**, *36*, 4863.

(4) Hansen, J.; Sato, M.; Ruedy, R.; Kharecha, P.; Lacis, A.; Miller, R.; Nazarenko, L.; Lo, K.; Schmidt, G. A.; Russell, G.; Aleinov, I.; Bauer, S.; Baum, E.; Cairns, B.; Canuto, V.; Chandler, M.; Cheng, Y.; Cohen, A.; Del Genio, A.; Faluvegi, G.; Fleming, E.; Friend, A.; Hall, T.; Jackman, C.; Jonas, J.; Kelley, M.; Kiang, N. Y.; Koch, D.; Labow, G.; Lerner, J.; Menon, S.; Novakov, T.; Oinas, V.; Perlwitz, J.; Rind, D.; Romanou, A.; Schmunk, R.; Shindell, D.; Stone, P.; Sun, S.; Streets, D.; Tausnev, N.; Thresher, D.; Unger, N.; Yao, M.; Zhang, S. *Climate Dynamics* **2007**, *29*, 661.

(5) Parrington, J. R.; Zoller, W. H.; Aras, N. K. *Science* **1983**, *220*, 195.

(6) Parrington, J. R. *Science* **1983**, *220*, 666.

(7) Neff, J. C.; Ballantyne, A. P.; Farmer, G. L.; Mahowald, N. M.; Conroy, J. L.; Landry, C. C.; Overpeck, J. T.; Painter, T. H.; Lawrence, C. R.; Reynolds, R. L. *Nature Geoscience* **2008**, *1*, 189.

(8) Prospero, J. M.; Barrett, K.; Church, T.; Dentener, F.; Duce, R. A.; Galloway, J. N.; Levy, H.; Moody, J.; Quinn, P. *Biogeochemistry* **1996**, *35*, 27.

(9) NASA Code 916, Atmospheric Chemistry and Dynamics Branch, Chinese Dust Storm, April 1998: http://toms.gsfc.nasa.gov/aerosols/china_1998.html.

(10) Usher, C. R.; Michel, A. E.; Grassian, V. H. *Chem. Rev.* **2003**, *103*, 4883.

(11) Zhang, Y.; Carmichael, G. R. *J. Appl. Meteorol.* **1999**, *38*, 353.

(12) Raes, F.; Bates, T.; McGovern, F.; Van Liedekerke, M. *Tellus Ser. B* **2000**, *52*, 111.

(13) de Reus, M.; Strom, J.; Curtius, J.; Pirjola, L.; Vignati, E.; Arnold, F.; Hansson, H. C.; Kulmala, M.; Lelieveld, J.; Raes, F. *J. Geophys. Res., [Atmos.]* **2000**, *105*, 24751.

(14) de Reus, M.; Dentener, F.; Thomas, A.; Borrmann, S.; Strom, J.; Lelieveld, J. *J. Geophys. Res., [Atmos.]* **2000**, *105*, 15263.

(15) Goddard Space Flight Center, Visible Earth, 2002. http://visibleearth.nasa.gov/Atmosphere/Aerosols/Dust_Ash.html.

(16) Gill, P. S.; Graedel, R. E.; Weschler, C. J. *Rev. Geophys.* **1983**, *21*, 903.

(17) Ellison, G. B.; Tuck, A. F.; Vaida, V. *J. Geophys. Res., [Atmos.]* **1999**, *104*, 11633.

(18) Laskin, A.; Gaspar, D. J.; Wang, W. H.; Hunt, S. W.; Cowin, J. P.; Colson, S. D.; Finlayson-Pitts, B. J. *Science* **2003**, *301*, 340.

(19) Stokes, G. Y.; Buchbinder, A. M.; Gibbs-Davis, J. M.; Scheidt, K. A.; Geiger, F. M. *J. Phys. Chem. A* **2008**, *112*, 11688.

(20) Stokes, G. Y.; Buchbinder, A. M.; Gibbs-Davis, J. M.; Scheidt, K. A.; Geiger, F. M. *Vib. Spectrosc.* **2009**, *50*, 86–98.

(21) Voges, A. B.; Stokes, G. Y.; Gibbs-Davis, J. M.; Lettan, R. B.; Bertin, P. A.; Pike, R. C.; Nguyen, S. T.; Scheidt, K. A.; Geiger, F. M. *J. Phys. Chem. C* **2007**, *111*, 1567.

(22) Eliason, T. L.; Aloisio, S.; Donaldson, D. J.; Cziczo, D. J.; Vaida, V. *Atmos. Environ.* **2003**, *37*, 2207.

(23) Eliason, T. L.; Gilman, J. B.; Vaida, V. *Atmos. Environ.* **2004**, *38*, 1367.

(24) Moise, T.; Rudich, Y. *J. Geophys. Res, [Atmos.]* **2000**, *105*, 14667.

(25) Thomas, E. R.; Frost, G. J.; Rudich, Y. *J. Geophys. Res., [Atmos.]* **2001**, *106*, 3045.

(26) Moise, T.; Rudich, Y. *J. Phys. Chem. A* **2002**, *106*, 6469.

(27) Rudich, Y. *Chem. Rev.* **2003**, *103*, 5097.

(28) Katrib, Y.; Martin, S. T.; Hung, H. M.; Rudich, Y.; Zhang, H. Z.; Slowik, J. G.; Davidovits, P.; Jayne, J. T.; Worsnop, D. R. *J. Phys. Chem. A* **2004**, *108*, 6686.

(29) Smith, G. D.; Woods, E.; DeForest, C. L.; Baer, T.; Miller, R. E. *J. Phys. Chem. A* **2002**, *106*, 8085.

(30) Hearn, J. D.; Smith, G. D. *J. Phys. Chem. A* **2004**, *108*, 10019.

(31) Hearn, J. D.; Lovett, A. J.; Smith, G. D. *Phys. Chem. Chem. Phys.* **2005**, *7*, 501.
(32) Hearn, J. D.; Smith, G. D. *J. Phys. Chem. A* **2007**, *111*, 11059.
(33) Usher, C. R.; Michel, A. E.; Stec, D.; Grassian, V. H. *Atmos. Environ.* **2003**, *37*, 5337.
(34) Thornberry, T.; Abbatt, J. P. D. *Phys. Chem. Chem. Phys.* **2004**, *6*, 84.
(35) Dubowski, Y.; Vieceli, J.; Tobias, D. J.; Gomez, A.; Lin, A.; Nizkorodov, S. A.; McIntire, T. M.; Finlayson-Pitts, B. J. *J. Phys. Chem. A* **2004**, *108*, 10473.
(36) Kwamena, N. O. A.; Earp, M. E.; Young, C. J.; Abbatt, J. P. D. *J. Phys. Chem. A* **2006**, *110*, 3638.
(37) Park, J.; Gomez, A. L.; Walser, M. L.; Lin, A.; Nizkorodov, S. A. *Phys. Chem. Chem. Phys.* **2006**, *8*, 2506.
(38) Poschl, U.; Letzel, T.; Schauer, C.; Niessner, R. *J. Phys. Chem. A* **2001**, *105*, 4029.
(39) Mang, S. A.; Henricksen, D. K.; Bateman, A. P.; Andersen, M. P. S.; Blake, D. R.; Nizkorodov, S. A. *J. Phys. Chem. A* **2008**, *112*, 8337.
(40) Voss, L. F.; Bazerbashi, M. F.; Beekman, C. P.; Hadad, C. M.; Allen, H. C. *J. Geophys. Res.* **2007**, *112*, D06209.
(41) Voss, L. F.; Hadad, C. M.; Allen, H. C. *J. Phys. Chem. B* **2006**, *110*, 19487.
(42) Seinfeld, J. H.; Pandis, S. N. *Atmospheric Chemistry and Physics*; John Wiley & Sons: New York, 1998.
(43) Daum, P. H.; Kleinman, L. I.; Springston, S. R.; Nunnermacker, L. J.; Lee, Y. N.; Weinstein-Lloyd, J.; Zheng, J.; Berkowitz, C. M. *J. Geophys. Res.* **2003**, *108*.
(44) Kleinman, L.; Lee, Y.-N.; Springston, S. R.; Nunnermacker, L.; Zhou, X.; Brown, R.; Hallock, K.; Klotz, P.; Leahy, D.; Lee, J. H.; Newman, L. *J. Geophys. Res., [Atmos.]* **1994**, *99*, 3469–3482.
(45) Hatakeyama, S.; Akimoto, H. *Res. Chem. Intermed.* **1994**, *20*, 503.
(46) Baker, J.; Aschmann, S. M.; Arey, J.; Atkinson, R. *Int. J. Chem. Kinet.* **2001**, *34*, 73.
(47) Fick, J.; Pommer, L.; Andersson, B.; Nilsson, C. *Atmos. Environ.* **2002**, *36*, 3299.
(48) Rickard, A. R.; Johnson, D.; McGill, C. D.; Marston, G. *J. Phys. Chem. A* **1999**, *103*, 7656.
(49) Fiegland, L. R.; McCorn Saint Fleur, M.; Morris, J. R. *Langmuir* **2005**, *21*, 2660.
(50) Karagulian, F.; Lea, A. S.; Dilbeck, C. W.; Finlayson-Pitts, B. J. *PCCP* **2008**, *10*, 528.
(51) Moussa, S. G.; McIntire, T. M.; Szori, M.; Roeselova, M.; Tobias, D. J.; Grimm, R. L.; Hemminger, J. C.; Finlayson-Pitts, B. J. *J. Phys. Chem. A* **2009**, *113*, 2060.
(52) Wade Jr., L. G. *Organic Chemistry*, 4th ed.; Printice Hall: Upper Saddle River, 1999.
(53) Vollhardt, K. P. C.; Schore, N. E. *Organic Chemistry: Structure and Function*, 3rd ed.; W. H. Freeman Company: New York, 1999.
(54) Bailey, P. S. *Ozonation in Organic Chemistry*; Academic Press: New York, 1978.
(55) Zhang, D.; Zhang, R. *J. Am. Chem. Soc.* **2002**, *124*, 2692.
(56) Gibbs-Davis, J. M.; Hayes, P. L.; Scheidt, K. A.; Geiger, F. M. *J. Am. Chem. Soc.* **2007**, *129*, 7175.
(57) Stokes, G. Y.; Boman, F. C.; Gibbs-Davis, J. M.; Stepp, B. R.; Condie, A.; Nguyen, S. T.; Geiger, F. M. *J. Am. Chem. Soc.* **2007**, *129*, 7492.
(58) Boman, F. C.; Musorrafiti, M. J.; Gibbs, J. M.; Stepp, B. R.; Salazar, A. M.; Nguyen, S. B. T.; Geiger, F. M. *J. Am. Chem. Soc.* **2005**, *127*, 15368.
(59) Boman, F. C.; Gibbs-Davis, J. M.; Heckman, L. M.; Stepp, B. R.; Nguyen, S. T.; Geiger, F. M. *J. Am. Chem. Soc.* **2009**, *131*, 844.
(60) Wedepohl, K. H. *Geochim. Cosmochim. Acta* **1995**, *59*, 1217.
(61) Cheng, S. S.; Scherson, D. A.; Sukenik, C. N. *Langmuir* **1995**, *11*, 1190.
(62) Kim, C. O.; Kim, D. H.; Kim, J. S.; Park, J. W. *Langmuir* **2006**, *22*, 4131.
(63) Demers, L. M.; Ginger, D. S.; Park, S. J.; Li, Z.; Chung, S. W.; Mirkin, C. A. *Science* **2002**, *296*, 1836.
(64) Allen, G. C.; Sorbello, F.; Altavilla, C.; Castorina, A.; Ciliberto, E. *Thin Solid Films* **2005**, *483*, 306.
(65) Anderson, A.; Ashurst, W. R. *Langmuir* **2008**, *24*, 7947.
(66) Vandenberg, E.; Elwing, H.; Askendal, A.; Lundstrom, I. *J. Colloid Interface Sci.* **1991**, *143*, 327.
(67) Vandenberg, E. T.; Bertilsson, L.; Liedberg, B.; Uvdal, K.; Erlandsson, R.; Elwing, H.; Lundstrom, I. *J. Colloid Interface Sci.* **1991**, *147*, 103.
(68) Butler, J. H.; Cronin, M.; Anderson, K. M.; Biddison, G. M.; Chatelain, F.; Cummer, M.; Davi, D. J.; Fisher, L.; Frauendorf, A. W.; Frueh, F. W.; Gjerstad, C.; Harper, T. F.; Kernahan, S. D.; Long, D. Q.; Pho, M.; Walker, J. A.; Brennan, T. M. *J. Am. Chem. Soc.* **2001**, *123*, 8887.
(69) Krasnoslobodtsev, A. V.; Smirnov, S. N. *Langmuir* **2002**, *18*, 3181.
(70) Heiney, P. A.; Gruneberg, K.; Fang, J. Y.; Dulcey, C.; Shashidhar, R. *Langmuir* **2000**, *16*, 2651.
(71) Kamisetty, N. K.; Pack, S. P.; Nonogawa, M.; Devarayapalli, K. C.; Kodaki, T.; Makino, K. *Anal. Bioanal. Chem.* **2006**, *386*, 1649.
(72) Voue, M.; Goormaghtigh, E.; Homble, F.; Marchand-Brynaert, J.; Conti, J.; Devouge, S.; De Coninck, J. *Langmuir* **2007**, *23*, 949.
(73) Zhang, F. X.; Srinivasan, M. P. *Langmuir* **2004**, *20*, 2309.
(74) Shen, Y. R. *The Principles of Nonlinear Optics*; John Wiley & Sons: New York, 1984.
(75) Zhu, X. D.; Suhr, H. J.; Shen, Y. R. *J. Opt. Soc. Am. B* **1986**, *3*, P252.
(76) Heinz, T. F. *Nonlinear Surface Electromagnetic Phenomena*; North-Holland: New York, 1991; Chapter 5.
(77) Boyd, R. W. *Nonlinear Opt.*; Academic Press: New York, 1992.
(78) Eisenthal, K. B. *Chem. Rev.* **1996**, *96*, 1343.
(79) Richmond, G. L. *Chem. Rev.* **2002**, *102*, 2693.
(80) Shen, Y. R.; Ostroverkhov, V. *Chem. Rev.* **2006**, *106*, 1140.
(81) Lambert, A. G.; Davies, P. B.; Neivandt, D. J. *Appl. Spectrosc. Rev.* **2005**, *40*, 103.
(82) van der Ham, E. W. M.; Vrehen, Q. H. F.; Eliel, E. R. *Surf. Sci.* **1996**, *368*, 96.
(83) Eliel, E. R.; van der Ham, E. W. M.; Vrehen, Q. H. F.; Barmentlo, M.; t Hooft, G. W.; van der Meer, A. F. G.; van Amersfoort, P. W. *Nucl. Instrum. Meth. A* **1994**, *341*, 152.
(84) Richter, L. J.; Petralli-Mallow, T. P.; Stephenson, J. C. *Opt. Lett.* **1998**, *23*, 1594.
(85) Hayes, P. L.; Chen, E. H.; Achtyl, J. L.; Geiger, F. M. *J. Phys. Chem. A* Accepted for publication.
(86) Esenturk, O.; Walker, R. A. *J. Phys. Chem. B.* **2004**, *108*, 10631.
(87) Calvert, J. G.; Atkinson, R.; Kerr, J. A.; Madronich, S.; Moortgat, G. K.; Wallington, T. J.; Yargood, G. *The Mechanisms of Atmospheric Oxidation of the Alkenes*; Oxford University Press: New York, 2000.
(88) Atkinson, R.; Arey, J. *Chem. Rev.* **2003**, *103*, 4605.
(89) Fenske, J. D.; Kuwata, K. T.; Houk, K. N.; Paulson, S. E. *J. Phys. Chem. A.* **2000**, *104*, 7246.
(90) Finlayson-Pitts, B. J.; Pitts Jr., J. N. *Chemistry of the Upper and Lower Atmosphere*; Academic Press: New York, 2000.
(91) March, J. *Advanced Organic Chemistry: Reactions, Mechanisms, and Structure*, 4th ed.; Wiley & Sons, Inc.: New York, 1992.
(92) Paulson, S. E.; Chung, M. Y.; Hasson, A. S. *J. Phys. Chem. A* **1999**, *103*, 8125.
(93) Paulson, S. E.; Orlando, J. J. *Geophys. Res. Lett.* **1996**, *23*, 3727.
(94) Aschmann, S. M.; Tuazon, E. C.; Arey, J.; Atkinson, R. *J. Phys. Chem. A* **2003**, *107*, 2247.
(95) Gao, S.; Keywood, M.; Ng, N. L.; Surratt, J.; Varutbangkul, V.; Bahreini, R.; Flagan, R. C.; Seinfeld, J. H. *J. Phys. Chem. A* **2004**, *108*, 10147.
(96) Varutbangkul, V.; Brechtel, F. J.; Bahreini, R.; Ng, N. L.; Keywood, M. D.; Kroll, J. H.; Flagan, R. C.; Seinfeld, J. H.; Lee, A.; Goldstein, A. H. *Atm. Chem. Phys.* **2006**, *6*, 2367.
(97) Vieceli, J.; Ma, O. L.; Tobias, D. J. *J. Phys. Chem. A* **2004**, *108*, 5806.
(98) Adamson, A. W.; Gast, A. P. *Physical Chemistry of Surfaces*, 6th ed.; John Wiley and Sons, Inc.: New York, 1997.
(99) Steinfeld, J. I.; Francisco, J. S.; Hase, W. L. *Chemical Kinetics and Dynamics*; Prentice Hall: Upper Saddle River, NJ, 1998.
(100) Ammann, M.; Poschl, U.; Rudich, Y. *Phys. Chem. Chem. Phys.* **2003**, *5*, 351.
(101) Poschl, U.; Rudich, Y.; Ammann, M. *Atm. Chem. Phys.* **2007**, *7*, 5989.
(102) Ammann, M.; Poschl, U. *Atm. Chem. Phys.* **2007**, *7*, 6025.
(103) Poeschl, U.; Letzel, T.; Schauer, C.; Niessner, R. *J. Phys. Chem. A* **2001**, *105*, 4029.
(104) Kwamena, N.-O. A.; Thornton, J. A.; Abbatt, J. P. D. *J. Phys. Chem. A* **2004**, *108*, 11626.
(105) McNeill, V. F.; Wolfe, G. M.; Thornton, J. A. *J. Phys. Chem. A* **2007**, *111*, 1073.
(106) Mmereki, B. T.; Donaldson, D. J. *J. Phys. Chem. A* **2003**, *107*, 11038.
(107) Eley, D. D.; Rideal, E. K. *Nature* **1940**, *146*, 401.
(108) Molina, M. J. *CHEMRAWN VII: Chemistry of the Atmosphere: The Impact of Global Change*; Blackwell Sci.: New York, 1994.
(109) Knopf, D. A.; Anthony, L. M.; Bertram, A. K. *J. Phys. Chem. A* **2005**, *109*, 5579.
(110) Rudich, Y.; Donahue, N. M.; Mentel, T. F. *Annu. Rev. Phys. Chem.* **2007**, *58*, 321.
(111) Schmidt, C. M.; Buchbinder, A. M.; Weitz, E.; Geiger, F. M. *J. Phys. Chem. A* **2007**, *111*, 13023.
(112) Schmidt, C. M.; Savara, A.; Weitz, E.; Geiger, F. M. *J. Phys. Chem. C* **2007**, *111*, 8260.
(113) Geiger, F. M. *Annu. Rev. Phys. Chem.* **2009**, *60*, 61.

JP904104S